AMERICAN SOCIETY FOR MICROBIOLOGY | Molecular and Cellular Biology

Occludin S471 Phosphorylation Contributes to Epithelial Monolayer Maturation

Mark T. Bolinger,[a,d] Aniket Ramshekar,[a] Helen V. Waldschmidt,[b] Scott D. Larsen,[b] Maria C. Bewley,[c] John M. Flanagan,[c] David A. Antonetti[a,d]

Department of Ophthalmology and Visual Sciences, Kellogg Eye Center, University of Michigan, Ann Arbor, Michigan, USA[a]; Vahlteich Medicinal Chemistry Core, Department of Medicinal Chemistry, College of Pharmacy, University of Michigan, Ann Arbor, Michigan, USA[b]; Departments of Biochemistry and Molecular Biology, Pennsylvania State University College of Medicine, Hershey, Pennsylvania, USA[c]; Department of Molecular and Integrative Physiology, University of Michigan, Ann Arbor, Michigan, USA[d]

Multiple organ systems require epithelial barriers for normal function, and barrier loss is a hallmark of diseases ranging from inflammation to epithelial cancers. However, the molecular processes regulating epithelial barrier maturation are not fully elucidated. After contact, epithelial cells undergo size-reductive proliferation and differentiate, creating a dense, highly ordered monolayer with high resistance barriers. We provide evidence that the tight junction protein occludin contributes to the regulation of epithelial cell maturation upon phosphorylation of S471 in its coiled-coil domain. Overexpression of a phosphoinhibitory occludin S471A mutant prevents size-reductive proliferation and subsequent tight junction maturation in a dominant manner. Inhibition of cell proliferation in cell-contacted but immature monolayers recapitulated this phenotype. A kinase screen identified G-protein-coupled receptor kinases (GRKs) targeting S471, and GRK inhibitors delayed epithelial packing and junction maturation. We conclude that occludin contributes to the regulation of size-reductive proliferation and epithelial cell maturation in a phosphorylation-dependent manner.

Cells characteristically form epithelial monolayers through logarithmic growth when cells are subconfluent followed by cell-to-cell contact and concluding with contact inhibition of proliferation (CIP), proliferative quiescence, and epithelial monolayer maturation, including tight junction (TJ) formation (1, 2). CIP is an important step in monolayer maturation that is mediated in part by the activation of the Hippo pathway. Hippo involves a signaling cascade with multiple mechanisms of regulation that may be initiated by homophilic interactions between extracellular domains of the adherens junction (AJ) protein E-cadherin on adjacent cells, ultimately leading to the exclusion of the transcriptional coactivator Yes-associated protein (YAP) from the nucleus (3, 4).

However, Puliafito et al. demonstrated that cell-cell contact is not sufficient for CIP in Madin-Darby canine kidney (MDCK) epithelial cells (2). In fact, proliferation continues at a near-subconfluent rate even in contacted cells until a critical cell density, or transition point, is reached, after which proliferation diminishes until cells reach quiescence (2, 5). Proliferation in contacted cells is accompanied by little or no hypertrophic growth. While subconfluent daughter cells ultimately attain nearly 100% of the mother cell area, confluent cells remain at ~50%, indicating a nearly complete lack of hypertrophic growth in the densely confluent monolayer, consistent with the previously identified inverse relationship between individual cell size and density (2, 6). This reduction in cell size acts as the major activator of YAP nuclear exclusion through a reduction of cytoskeletal stress (7, 8). Indeed, a forced reduction in cell size by growth on micropatterned fibronectin islands of a defined area or growth in soft agar, to reduce cytoskeletal tension, leads to YAP exclusion in a manner dependent on F-actin-capping/severing proteins but independent of cell contact (7). Thus, subconfluent cells are subjected to tensile forces on the cytoskeleton that, combined with a lack of cell contact, promote YAP nuclear localization and proliferation (7–9). Confluent, pre-transition-point epithelial cells, while contacted, also maintain YAP nuclear localization due to continued cytoskeletal tension, promoting proliferation. However, the cells are exposed to constraining forces that discourage postmitotic hypertrophic growth, causing a period of size-reductive proliferation, ultimately reducing cytoskeletal stress and transitioning the cells to proliferative quiescence and, finally, monolayer maturation (2). This process sharply decreases cell area and increases cell density, resulting in increased uniformity of cell area and shape, and establishes a mature, packed, epithelial monolayer.

A mature epithelial monolayer possesses well-developed TJs, which are necessary to control fluid and solute flux. TJs form between adjacent cells apical to the AJ, create and maintain semipermeable barriers to paracellular flux, and may contribute to maintaining cell polarity. Over 40 proteins have been identified at TJs (10), including occludin (Occ), the first transmembrane TJ protein to be discovered (11). While occludin knockout mice failed to exhibit any increase in intestinal permeability, these animals presented with a constellation of complex phenotypes consistent with barrier dysregulation, including male sterility, an inability to nurse, and brain calcification (12, 13). Human patients expressing a recessive mutation in the occludin gene exhibit similar brain calcification as well as gross cranial malformation (14).

Received 22 January 2016 **Returned for modification** 19 February 2016
Accepted 10 May 2016

Accepted manuscript posted online 16 May 2016

Citation Bolinger MT, Ramshekar A, Waldschmidt HV, Larsen SD, Bewley MC, Flanagan JM, Antonetti DA. 2016. Occludin S471 phosphorylation contributes to epithelial monolayer maturation. Mol Cell Biol 36:2051–2066. doi:10.1128/MCB.00053-16.

Address correspondence to David A. Antonetti, dantonet@umich.edu.

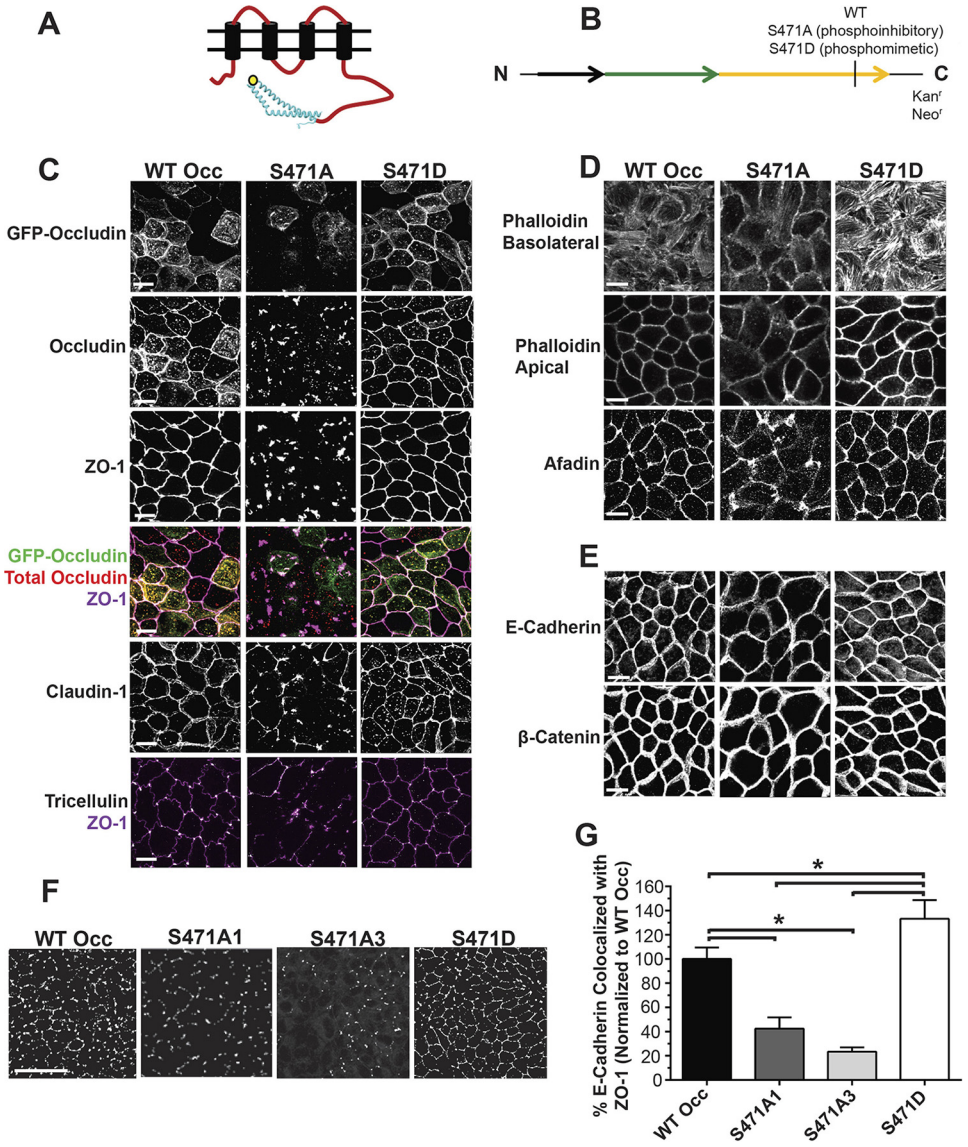

FIG 1 TJ and cytoskeletal proteins are mislocalized in occludin S471A mutant-expressing cell lines. (A and B) Schematic of occludin with the S471 site (yellow dot) (A) and fusion protein construct with mutations used for stable expression in MDCK cell lines (B). (C to E) Immunofluorescence maximum projected stacks (3 μm thick) or slices (phalloidin images only, 0.5 μm thick) of the indicated TJ (C), cytoskeletal and afadin (D), and AJ (E) proteins at 4 days postconfluence (bars = 10 μm). (F) Maximum projected colocalization of E-cadherin, used as a marker of the junctional complex, with ZO-1, demonstrating the loss of ZO-1 at junctions (bar = 50 μm). (G) Quantification of data shown in panel F (averages from 4 images per cell line). Data are expressed as means ± SD. *, $P < 0.05$ compared to WT Occ or S471D Occ.

Taken together, these studies support the prevailing view of occludin as a regulator of the TJ.

Recently, occludin has been increasingly implicated in nonbarrier roles, including the regulation of cell proliferation. Occludin is present at centrosomes and regulates mitotic entry and cell proliferation in a phosphorylation-dependent manner (15). Occludin knockout mice exhibit intestinal cell hyperplasia (12), and occludin downregulation or loss has been implicated in cancers of the skin (16), uterus (17), and breast (18) and is correlated with increased metastatic potential (19). Furthermore, occludin reexpression rescues murine tumorigenesis after implantation of oncogenic, Raf1-transformed cells (20). The emerging importance of occludin in cell proliferation, particularly in tumors of the confluent epithelium, suggests a possible role in high-confluence proliferation and, by extension, in cell packing.

Mass spectrometric analysis has identified several novel occludin phosphorylation sites, including the S471 site within the C-terminal coiled-coil domain (21). Notably, this residue is located at the first turn of the coiled coil, which has been established as a point of interaction with the scaffolding protein zonula occludens 1 (ZO-1) (22). ZO-1 interacts with and organizes many TJ proteins and links the junction to the actin cytoskeleton (23), and members of the ZO family are necessary for the assembly of TJs (24, 25). ZO-1 is a membrane-associated guanylate kinase (MAGUK) protein and contains the typical catalytically inactive guanylate kinase (GuK)-like domain. The GuK domain acts as a

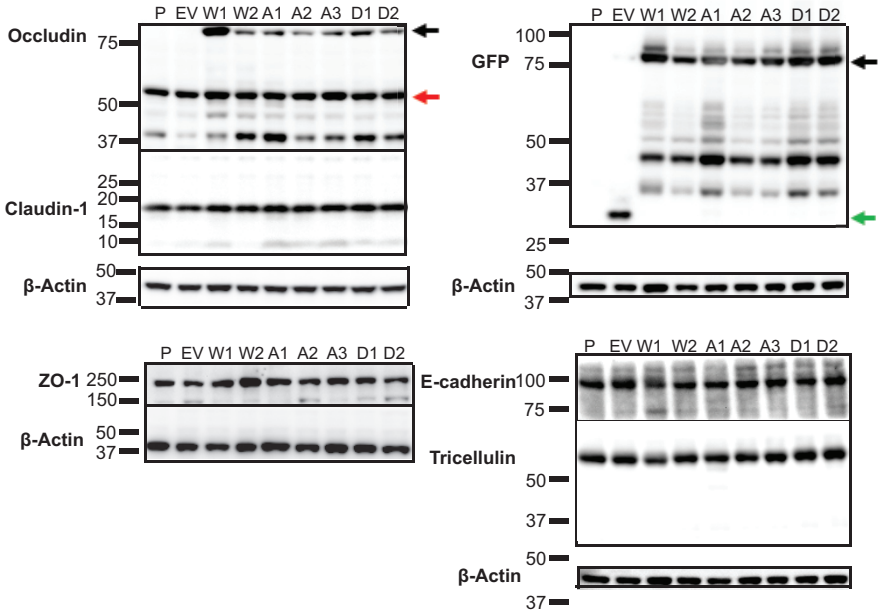

FIG 2 S471 point mutations do not affect tight junction protein content. Shown are Western blots for the indicated TJ and AJ proteins. P, parental; EV, empty vector; W1 and W2, WT Occ clones 1 and 2; A1 to A3, S471A Occ clones 1 to 3, D1 and D2, S471D Occ clones 1 and 2. Arrows indicate exogenous GFP-occludin (black), endogenous occludin (red), and GFP (green). All molecular markers are given in kilodaltons. W2, A3, and D2 lines were used unless otherwise indicated.

specialized P-serine/P-threonine binding pocket (26), and the ZO-1 GuK domain interacts with the acidic head of the occludin coiled coil, including the S471 site, making it an intriguing site for potential functional regulation and further analysis (22).

In the present study, we present evidence that the expression of the occludin S471A phosphoinhibitory mutant prevents size-reductive proliferation and cell packing in MDCK cells. Expression of the S471A mutant has no effect on subconfluent proliferation but inhibits size-reductive proliferation after contact and prevents bicellular and tricellular TJ maturation, creating a highly permeable monolayer that appears morphologically indistinguishable from an immature monolayer before cell packing. Furthermore, inhibition of cell cycle progression after cell contact yields a similar, immature monolayer, suggesting that cell packing is necessary for monolayer maturation and TJ formation. The S471 site is a target of members of the G-protein-coupled receptor kinase (GRK) family, and inhibition of GRK4-6 also inhibits size-reductive proliferation and delays epithelial cell maturation. Furthermore, the effect of the GRK inhibitors on monolayer maturation can be overcome by the expression of the phosphomimetic S471D occludin mutant. The data suggest that occludin phosphorylation at S471 contributes to the control of size-reductive proliferation after contact and to epithelial cell maturation.

MATERIALS AND METHODS

Cells. All reagents were purchased from Sigma Chemical (St. Louis, MO) unless otherwise noted. MDCK cells were obtained from the American Type Culture Collection (Manassas, VA) and cultured in minimum essential medium (MEM) as previously reported (15). All cells were kept at 37°C with 5% CO_2.

MDCK stable lines were generated via transfection with Lipofectamine 2000 (Invitrogen, Carlsbad, CA) of an empty vector, wild-type human occludin, the S471A occludin mutant, or the S471D occludin mutant in a pmaxFP expression vector (Amaxa, Cologne, Germany) according to the manufacturer's instructions and as previously described (27).

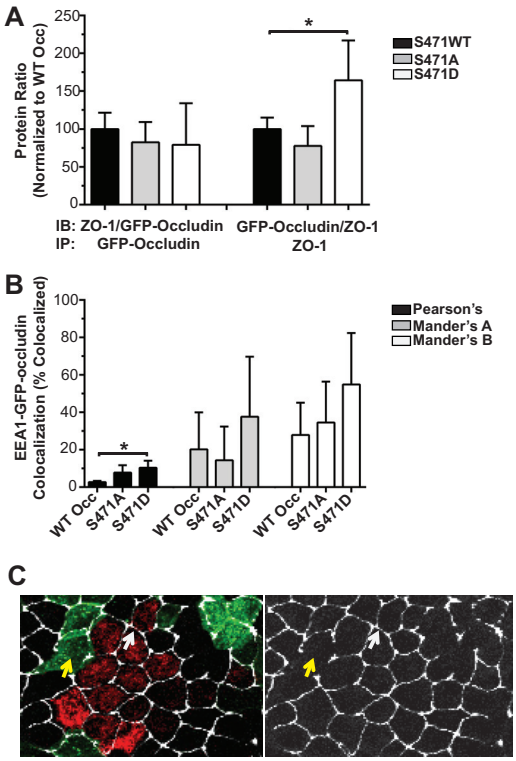

FIG 3 Coimmunoprecipitation, colocalization, and cocultures. (A) Protein ratio of coimmunoprecipitation for GFP-occludin and ZO-1 normalized to the WT Occ protein ratio ($n = 5$ to 6). IB, immunoblotting; IP, immunoprecipitation. (B) Colocalization of GFP-occludin and the endosomal marker EEA1 (averages from 3 to 5 images per condition). Data are expressed as means ± SD. *, $P < 0.05$ compared to WT Occ. (C) Parental cells were labeled with CellLight Mitochondria BacMam baculovirus (red) and then cocultured with GFP-tagged S471A Occ-expressing lines (green) and stained for ZO-1 (faux colored white). Left, merged image; right, ZO-1 alone. Arrows indicate intact parental-parental (white) and disrupted S471A-S471A (yellow) borders.

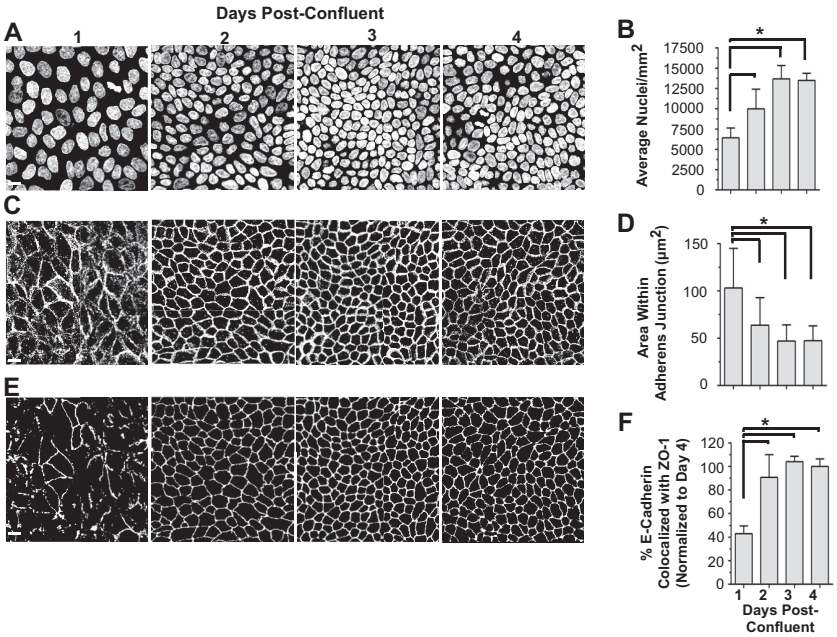

FIG 4 Size-reductive proliferation and TJ organization in MDCK cells. Cell number, size, and junctional organization were quantified 1 to 4 days following high-confluence plating. Images and quantifications are shown for nuclei (DAPI [4′,6-diamidino-2-phenylindole]) (A and B), E-cadherin IF and area within the AJ (C and D), and ZO-1 IF and the maximum projected colocalization with E-cadherin as a measure of ZO-1 border continuity and TJ assembly (E and F) (bars, 10 μm). In panel F, data are expressed as means ± SD (averages from 4 images per condition). *, $P < 0.05$ compared to 1 day postconfluence.

Briefly, fluorescence-activated cell sorting was carried out following 2 weeks of culture in normal MEM with 2.5 mg/ml Geneticin (Gibco, Carlsbad, CA). Single cells were plated in a 96-well plate with 2.5 μl/ml Geneticin, grown out, and screened for green fluorescent protein (GFP) expression by Western blotting. W2, A3, and D2 lines were used unless otherwise indicated.

All reported experiments were repeated on separate days except for experiments shown in Fig. 4, which represent multiple platings. Cells were plated at a density of 162,500 cells/cm^2 unless otherwise noted.

Immunofluorescence (IF). Cells were plated onto chambered glass slides and fixed at 4 days postconfluence, unless otherwise noted, with either 3.5% paraformaldehyde (PFA) for 10 min or 50% methanol–50% acetone for 20 min at −20°C (Thermo Scientific, Waltham, MA). PFA fixation was followed by 15 min of permeabilization in Tris-buffered saline (TBS) plus 0.25% Triton X-100, while methanol-acetone fixation did not require permeabilization. Cells were blocked in 10% goat serum (Life Technologies, Carlsbad, CA) with 0.25% Triton X-100 for 1 h and then stained with the indicated primary antibodies overnight at 4°C at a 1:200 dilution in blocking solution, except for anti-turbo GFP (1:400), anti-YAP (1:100), and anti-GRK (1:100). Secondary antibody (Alexa Fluor 488, 555, and 647; Life Technologies, Carlsbad, CA) exposure was done for 1 h at room temperature in blocking buffer at a 1:1,000 dilution. Fluorescence was determined from z-stacks of 0.5-μm slices taken on a Leica TCS SP5 confocal microscope (63×, 1.4-numerical-aperture [NA] oil objective; Wetzlar, Germany) with photomultiplier tube detectors and by using Leica Advanced Fluorescence software. Images were analyzed by using Metamorph software (Molecular Devices, Sunnyvale, CA). In some cases, occludin and ZO-1 border staining was quantified by a semiquantitative ranking score system based on a scale of 1 to 5: 1 for the near-complete loss of border staining (0 to 25%), 2 for 25 to 50% continuous border staining, 3 for 50 to 75% continuous border staining, 4 for 75 to 100% continuous border staining, and 5 for completely continuous border staining. Scoring was completed in a masked fashion by 3 impartial observers provided scoring standard images for comparison.

Cell counts. Nuclei were counted from monolayers stained with either Hoechst or PicoGreen nuclear stain (Life Technologies, Carlsbad, CA) by

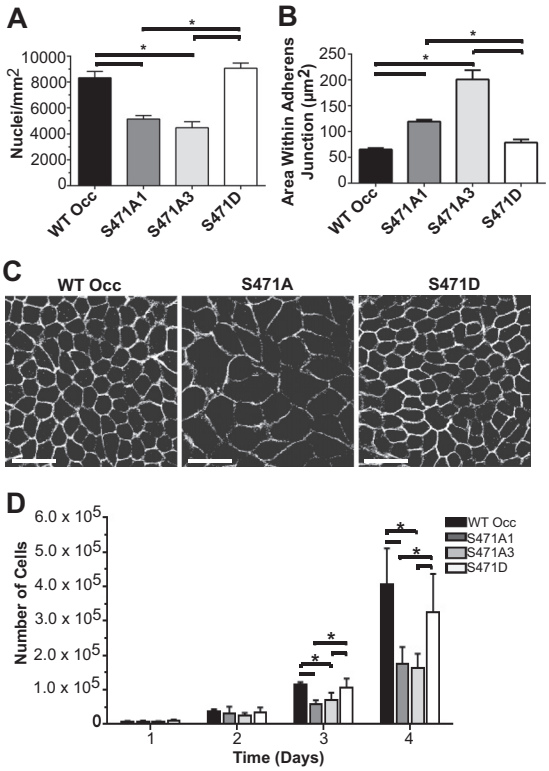

FIG 5 Phosphoinhibitory (S471A) monolayers are composed of fewer, larger cells than WT Occ- or S471D mutant-expressing monolayers. (A and B) Quantification of nuclei per area (A) and area within the AJ (E-cadherin staining) (B) of 4-day-postconfluent monolayers in various cell lines. (C) Representative E-cadherin staining (bars = 10 μm). (D) Cell counts by flow cytometry at 1, 2, 3, or 4 days postplating at low confluence. Data are expressed as means ± SD (averages from 4 images per condition [A and B] and $n = 9$ [D]). *, $P < 0.05$ compared to WT Occ or S471D Occ.

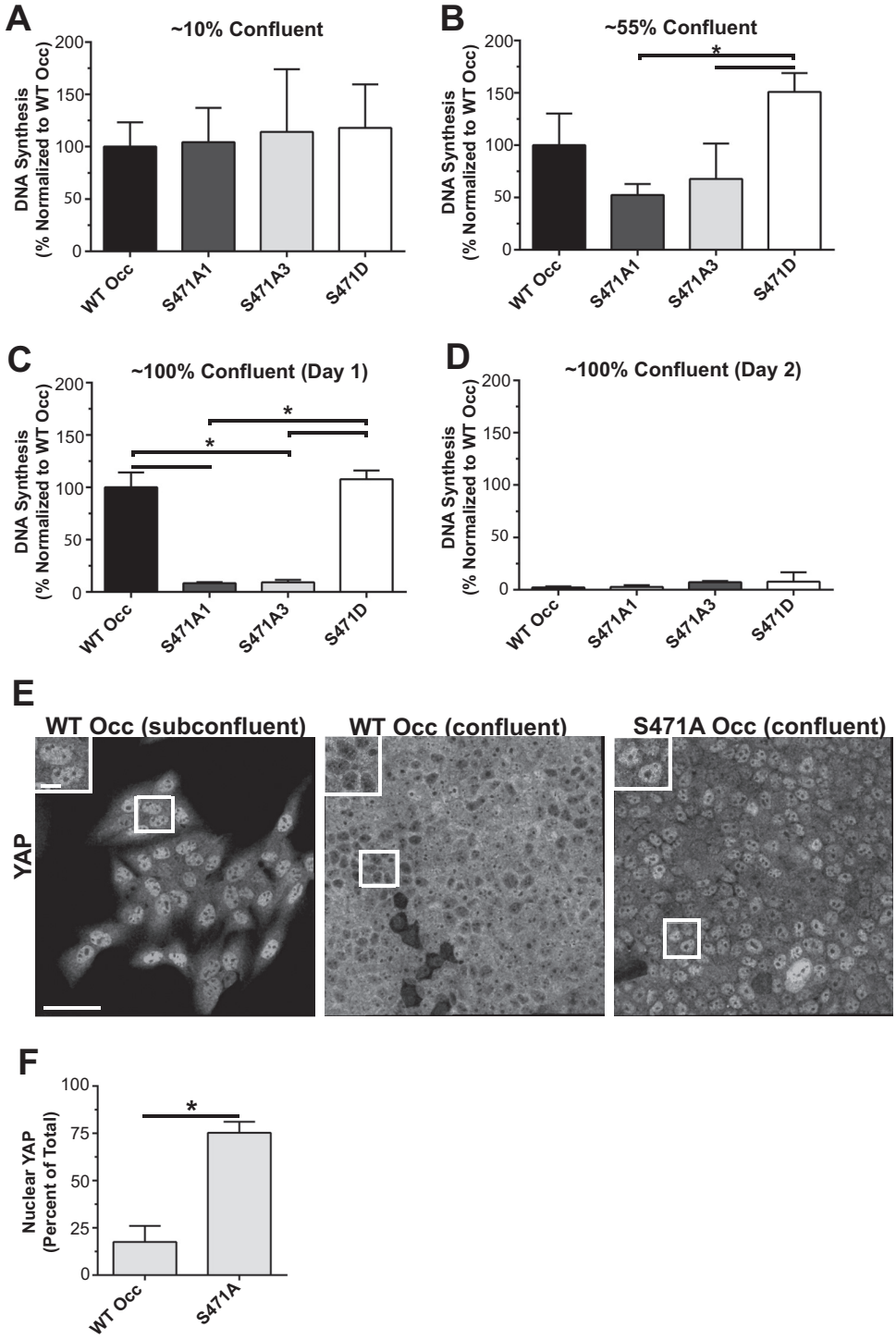

FIG 6 Proliferation after contact was inhibited in S471A Occ-expressing lines. (A to D) EdU labeling was measured at the indicated confluences as described in Materials and Methods, and the percentage of cells demonstrating DNA synthesis was quantified (at least 500 cells were examined per cell line, per condition). (E) Representative IF images of YAP localization in subconfluent and confluent WT Occ-expressing and confluent S471A Occ-expressing lines (bar = 50 μm [10 μm for inset]). (F) Quantification of the percentage of nuclear YAP (averages from 4 images per condition). Data are expressed as means ± SD normalized to WT Occ. *, $P < 0.05$ compared to WT Occ.

using the ImageJ cell counter plug-in (NIH, Bethesda, MD). Data from at least four microscopy fields were averaged for each cell line or treatment (63× objective, 5× zoom). A total of 1,400 cells/cm^2 were also plated onto 12-well plates and then trypsinized and counted at 1, 2, 3, and 4 days postplating by using a Mo-FLO cell sorter (Beckman Coulter, Brea, CA). Forward-scatter data were collected to determine suspended-cell sizes.

DNA synthesis/cell proliferation assays. A total of 7,857, 100,000, or 185,714 cells/cm^2 were plated onto eight chambered glass slides (Thermo

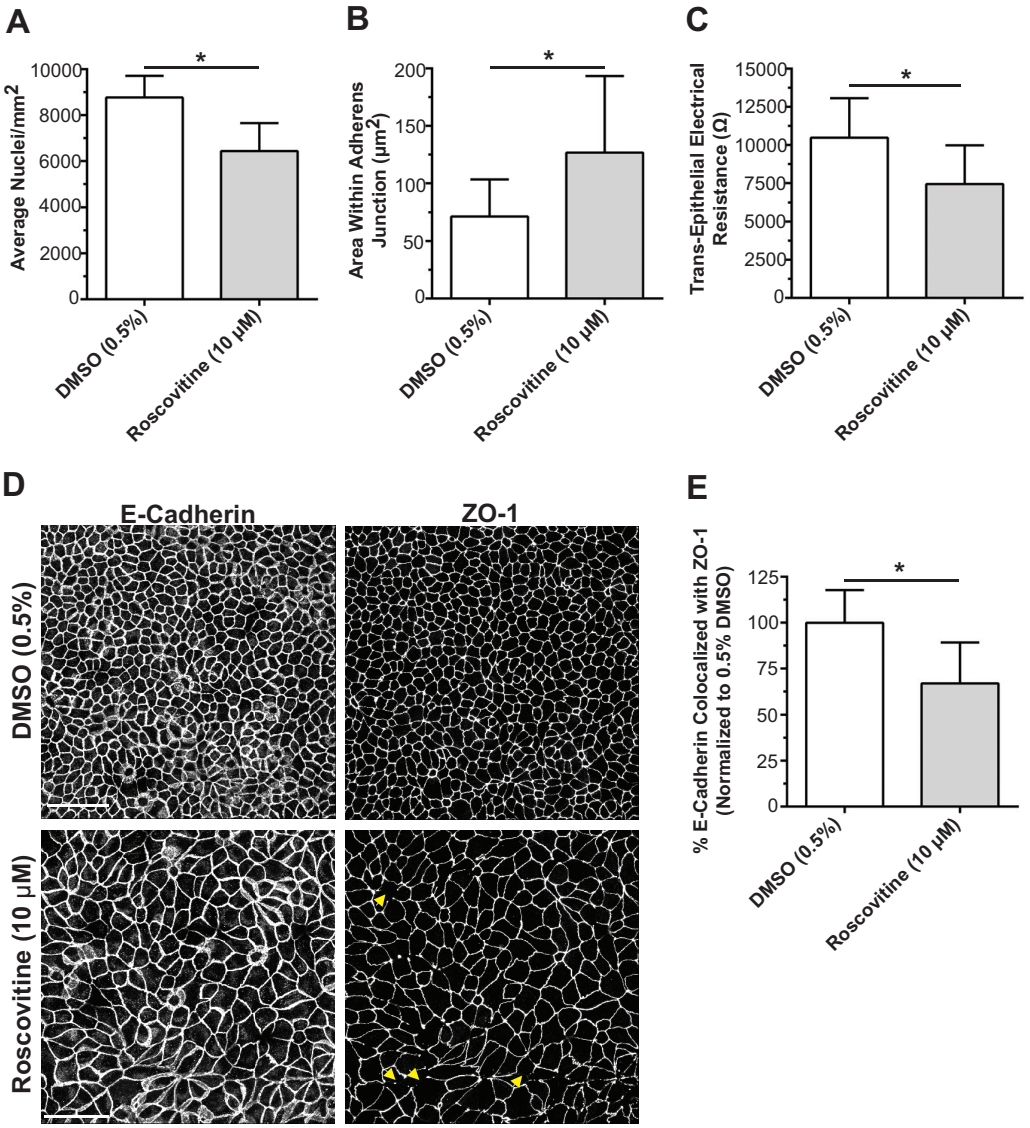

FIG 7 Inhibition of size-reductive proliferation results in delayed peak TER and TJ protein mislocalization. (A and B) Nucleus counts (A) and AJ area (B) in day 3 postconfluent MDCK monolayers demonstrating inhibition of size-reductive proliferation following treatment with the cell cycle inhibitor roscovitine added 24 h after plating. (C) TER of day 3 postconfluent MDCK cells ($n = 10$ or 11). (D) Representative IF images of E-cadherin (AJ marker) and ZO-1 (TJ marker) following treatment with roscovitine or the DMSO control (bar, 50 μm). Arrows highlight gaps in ZO-1 at the border. (E) Quantification of the maximum projected colocalization of ZO-1 with E-cadherin as a measure of ZO-1 border continuity and TJ assembly. Data are expressed as means ± standard deviations (averages from 4 images per condition). *, $P < 0.05$ compared to 0.5% DMSO.

Scientific, Waltham, MA) and allowed to grow overnight (7,857 and 100,000 cells/cm^2) or for 4 h (185,714 cells/cm^2). Cells were incubated with 10 μM 5-ethynyl-2′-deoxyuridine (EdU) (Click-It EdU kit; Life Technologies, Carlsbad, CA) for 4 h (7,857 and 100,000 cells/cm^2) or 24 h (185,714 cells/cm^2) according to the manufacturer's instructions. Cells were fixed with 3.5% PFA and stained with Hoechst or PicoGreen nuclear stain (Invitrogen, Carlsbad, CA). At least 500 cells per condition were examined by using the ImageJ cell counter plug-in (NIH, Bethesda, MD), and the percentage of total cells expressing EdU was calculated.

Transepithelial resistance. Transepithelial resistance (TER) was determined by using an electric cell-substrate impedance sensing (ECIS) system (Applied Biophysics, Troy, NY) at 500 Hz. Cells were plated on 8W10E$^+$ ECIS plates and allowed to become confluent overnight. All treatments were added at the time of plating and replenished along with fresh medium every 24 h unless otherwise noted. Electrical resistance was determined on the fourth day postconfluence unless otherwise noted.

Solute flux assay. Cells were plated onto 12-well plates with polyester Transwell inserts (0.4 μM pore; Corning, Corning, NY) and allowed to become confluent overnight. Solute flux was determined on the fourth day postconfluence as previously described (28). Briefly, 480 nM 6-carboxytetramethylrhodamine (TAMRA) (467 Da) was added to the apical chamber, followed by sampling of 50 μl from the basolateral chamber every 30 min for 3 h. Ten microliters was also removed from the apical chamber at the last time point for apical concentration determination. Fluorescence was measured (excitation at 560 nm and emission at 590 nm) in a flat-bottom black-wall 96-well plate (Greiner, Monroe, NC) by using a FLUOstar microplate reader (BMG Labtech, Ortenburg, Germany).

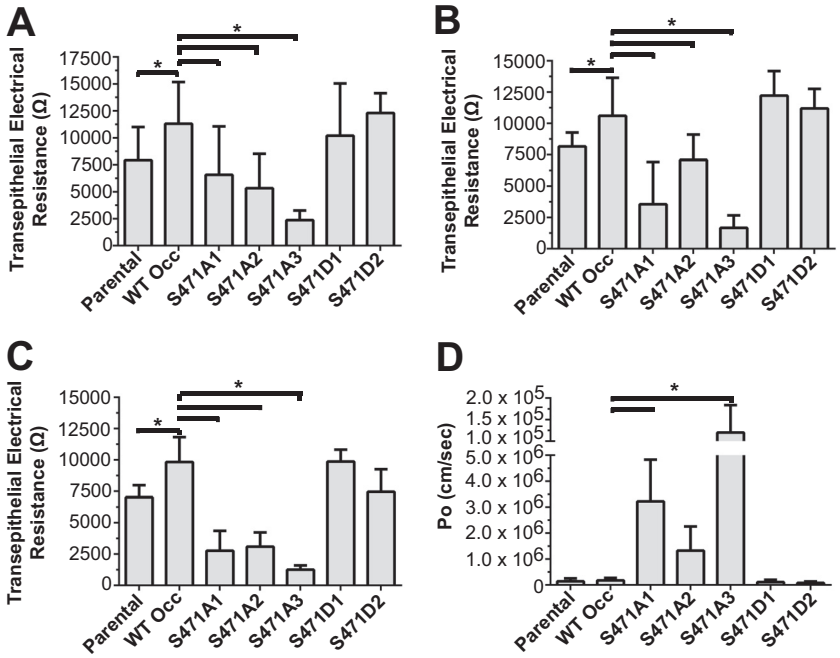

FIG 8 Barrier permeability is increased in phosphoinhibitory S471A Occ-expressing lines compared to WT Occ- or S471D mutant-expressing lines. (A to C) TER at 3 days (A) or 4 days (B) postconfluence or following 12 h of recovery from a day 4 calcium switch experiment (C). (D) Solute flux of a TAMRA tracer (467 Da) at 4 days postconfluence. Data are expressed as means ± SD ($n = 9$ to 16 [A to C] and $n = 13$ to 21 [D]). *, $P < 0.05$ compared to WT Occ.

Cell cycle inhibitor assays. Cells were treated with 10 μM roscovitine (Calbiochem, San Diego, CA) 24 h after plating. Drug was replenished along with fresh medium every 24 h, and TER measurements proceeded for two additional days (ECIS), or cells were fixed for imaging at 60 h postplating.

Kinase screen. A list of potential kinases was compiled by entering the sequence around S471 (KELDDYREESEEYMAAADE) into three online kinase prediction programs: GPS (29), KinasePhos (30), and NetPhos (31). Kinases predicted to phosphorylate S471 by at least two of the three programs were included in an *in vitro* ^{32}P kinase assay (Millipore, Dundee, Scotland, United Kingdom) of the same peptide with two added lysines at the amino terminus to promote peptide capture on nitrocellulose filters (KKKELDDYREESEEYMAAADE; NeoBioSci, Cambridge, MA). GRK identified in this screen was inhibited in MDCK cells by using the kinase-specific inhibitors CCG215022 (GRK inhibitor 22 [GRK Inhib 22]) (32), 4-amino-5-(bromomethyl)-2-methylpyrimidine hydrobromide (ABMH; Santa Cruz), and paroxetine (Toronto Research Chemicals, Toronto, ON, Canada). Kinase assays with all three inhibitors were performed exactly as previously reported (32).

Immunoprecipitation and Western blotting. Protein expression was determined via Western blotting as previously described (28). Briefly, MDCK cells were harvested in Stuart's buffer composed of 100 mM NaCl, 1% Triton X-100, 0.5% sodium deoxycholate, 0.2% SDS, 2 mM EDTA, 10 mM HEPES (pH 7.5), 1 mM $NaVO_4$, 10 mM NaF, 10 mM sodium pyrophosphate, 1 mM benzamidine, 10 μM microcystin (Cayman Chemical, Ann Arbor, MI), and a Complete Mini protease inhibitor tablet (EDTA free; Roche, Indianapolis, IN). Following gel electrophoresis and blocking in 2% ECL prime (GE Healthcare, Little Chalfont, Buckinghamshire, United Kingdom), proteins were probed with the indicated antibodies, including occludin, claudin-1, and tricellulin (Invitrogen, Carlsbad, CA); β-catenin and afadin (Sigma, St. Louis, MO); turbo GFP (Evrogen, Moscow, Russia); ZO-1 (Millipore, Billerica, MA); and E-cadherin (BD Biosciences, Franklin Lakes, NJ). Alternatively, MDCK cells were harvested for immunoprecipitation, as previously described (33), in buffer containing 50 mM Tris (pH 7.5), 150 mM NaCl, 1% NP-40 (USB, Cleveland, OH), 1 mM $NaVO_4$, 10 mM NaF, 10 mM sodium pyrophosphate, 1 mM benzamidine, Complete Mini protease inhibitor tablet (EDTA free; Roche, Indianapolis, IN), 1 μM microcystin (Cayman Chemical, Ann

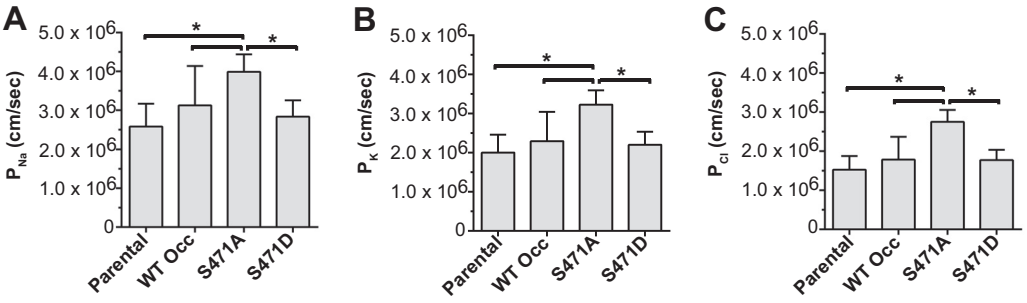

FIG 9 Permeability to multiple ions is increased in S471A mutant-expressing lines. Shown is ion permeability for sodium (A), potassium (B), and chloride (C) in day 4 postconfluent parental and various S471 mutant-expressing MDCK lines. Data are expressed as means ± SD ($n = 9$ per condition). *, $P < 0.05$ compared to the S471A mutant.

Arbor, MI), 10% glycerol (Fisher, Waltham, MA), and 2 mM EDTA (Lonza, Walkersville, MD). Following harvest, cells were rocked for 15 min and spun at 12,000 × *g* for 10 min. The lysate containing 1 mg of protein was precleared with a 30-μl packed volume of protein G-Sepharose beads (GE Healthcare, Little Chalfont, Buckinghamshire, United Kingdom) and then incubated overnight with 10 μg turbo GFP antibody (Evrogen, Moscow, Russia). Protein G beads were added to the mixture of the antibody and lysate for 1 h and then washed with buffer and prepared for Western blotting as described above.

Coculture experiments. Subconfluent parental MDCK cells were transduced with Cell-Light Mitochondria BacMam baculovirus (Invitrogen, Carlsbad, CA). The next day, transduced parental MDCK cells were plated with untransduced S471A Occ cells at a ratio of 10%/90%, respectively. Cells were fixed in PFA and prepared for IF as described above.

Ion permeability. Cells were plated onto Biopore cell culture inserts (0.4-μm pore; Millipore, Billerica, MA), with fresh MDCK medium being provided daily. On the fourth day postconfluence, inserts were loaded into an Ussing chamber (Harvard Apparatus, Holliston, MA), and both sides were gently filled with HEPES Ringer solution composed of 135 mM NaCl, 5 mM KCl, 10 mM HEPES, 10 mM glucose, 1.8 mM $CaCl_2$, and 1 mM $MgCl_2$. Permeability to specific ions was determined exactly as described previously by Hou et al. (EC-800 amplifier; Warner Instruments, Hamden, CT), except that the concentration of ions of interest (NaCl or KCl) in Ringer solution was reduced to 25% of the original concentration, and all experiments were conducted at 22°C (34).

Cell viability. Cell viability was determined by using a WST-1 assay (Roche, Indianapolis, IN). A total of 31,250 cells/cm^2 were plated into a 96-well plate, allowed to grow overnight, and then incubated with 5 μl WST-1 reagent for 1 h. Absorbance was measured (770/410 nm) by using a FLUOstar microplate reader (BMG Labtech, Ortenburg, Germany).

Statistical analysis. Data were analyzed by using two-tailed Student's *t* test (2 groups) or one-way analysis of variance (ANOVA) with a Bonferroni *post hoc* test (3 or more groups) by using Prism 5.0 (GraphPad Software, La Jolla, CA). Line graphs were analyzed by using a two-way ANOVA (simple effect within rows) with Bonferroni *post hoc* analysis. Data are expressed as means ± standard deviations (SD) unless otherwise indicated.

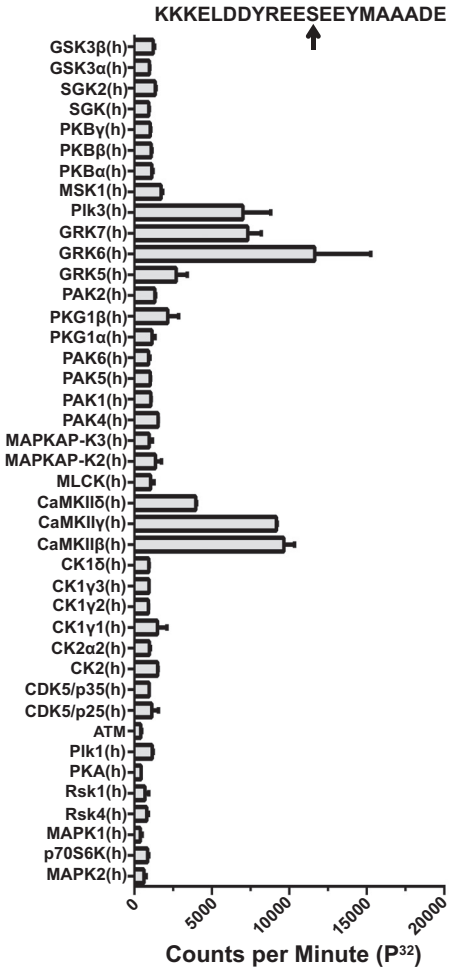

FIG 10 S471 *in vitro* kinase screen. Phosphorylation of an S471-containing 21-amino-acid peptide by the indicated kinases was quantified via ^{32}P incorporation. The peptide sequence with the location of S471 (arrow) is given.

RESULTS

S471A Occ expression compromises TJ protein organization. MDCK lines overexpressing human occludin with a phosphoinhibitory serine-to-alanine (S471A) or phosphomimetic serine-to-aspartic acid (S471D) mutation were generated along with wild-type occludin (WT Occ) control lines to investigate the effect of S471 phosphorylation on TJ protein organization (Fig. 1A and B). Both exogenous GFP-tagged occludin (80 kDa) and endogenous occludin (55 kDa) were detectable by Western blotting, and no appreciable changes were observed for the expression of any tested TJ or AJ proteins in lines utilized for the present study (Fig. 2). Cells expressing WT Occ had a well-organized localization at the border for the TJ proteins occludin (GFP-occludin and total occludin), ZO-1, and claudin-1 based on immunofluorescence (IF) labeling (Fig. 1C). Additionally, tricellulin appeared at tricellular junctions. Phalloidin staining for F-actin revealed stress fibers basolaterally and crisp cortical actin staining apically, while afadin was present at the border (Fig. 1D). Finally, the AJ proteins E-cadherin and β-catenin demonstrated strong cell border organization (Fig. 1E). All results were consistent with the known localization of these proteins in cells with high electrical resistance and low solute permeability. S471D Occ-expressing cells were similar to control lines in their staining patterns and in many cases were qualitatively better organized, with increased uniformity in cell shape and brighter, more focused border staining, particularly in regard to cortical F-actin (Fig. 1C to E). In contrast, TJs were disorganized in S471A Occ-expressing lines, with mislocalized or missing border staining in all examined TJ proteins. These studies were performed on day 4 after plating, and TJ disorganization was maintained for at least 10 days after plating. The TJ proteins occludin, ZO-1, and claudin-1 appeared as noncontinuous aggregates, often colocalizing with each other, while tricellulin staining was largely absent (Fig. 1C). S471A Occ expression did not, however, decrease the occludin–ZO-1 interaction, as judged by coimmunoprecipitation experiments (Fig. 3A), or alter the colocalization with early endosome antigen 1 (endosome marker) (Fig. 3B), nor was there evidence that S471A mutant cells corrupted the neighboring parental cell TJ organization (Fig. 3C), suggesting a cell-autonomous effect. In contrast, F-actin staining was altered, with fewer visible stress fibers and a dim, broad, cortical actin organization. Afadin was also disorganized or lost at bicellular junctions (Fig. 1D), but importantly, the AJ proteins E-cadherin and β-catenin appeared unaffected (Fig. 1E). To quantify the extent of ZO-1 protein mislocalization, colocalization between ZO-1, a marker of TJ organization, and E-cadherin, an AJ protein unaffected by S471A Occ expression, was measured. The percentage of E-cadherin colocalized with ZO-1 (indicating ZO-1 border

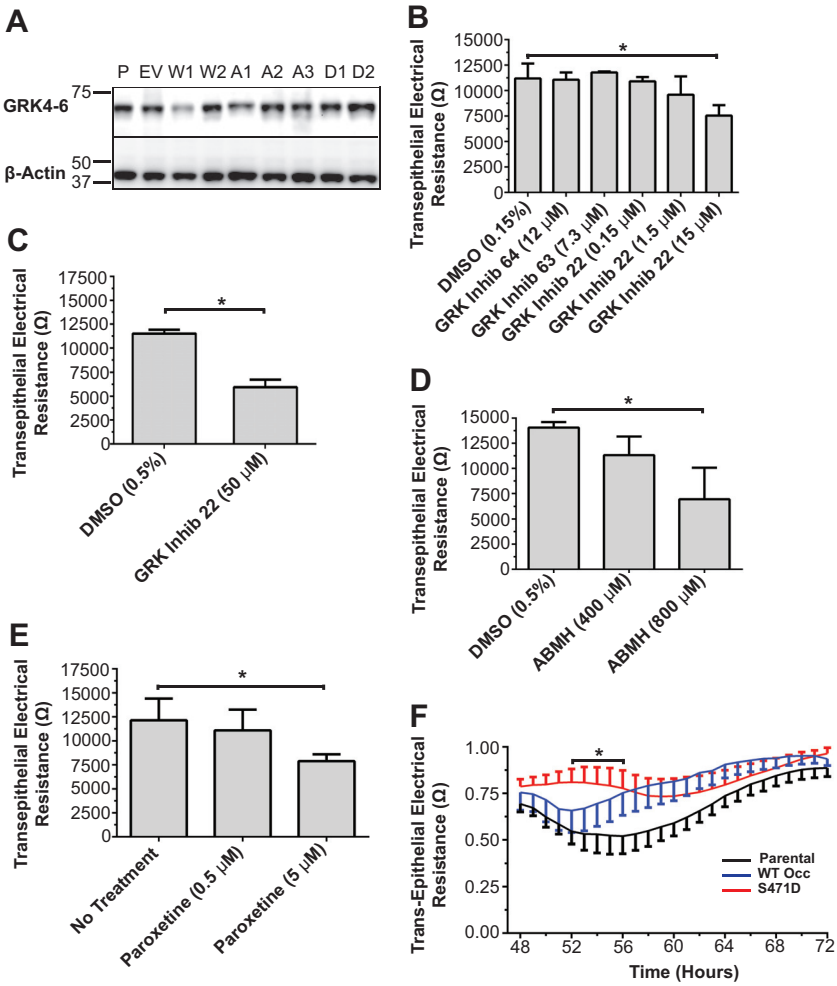

FIG 11 GRK inhibitors reduce TER in a dose-dependent manner. (A) Western blotting of all lines showing GRK4-6 expression. (B to E) TER at 3 days postconfluence of MDCK cells treated from the beginning of each experiment with various GRK inhibitors, including GRK inhibitors 64, 63, and 22 (15 μM) (B); GRK inhibitor 22 (50 μM) (C); ABMH (D); and paroxetine (E). Data are expressed as means ± SD ($n = 4$ to 8), *, $P < 0.05$ compared to the control. (F) Day 3 TER following treatment with GRK Inhib 22, normalized to the DMSO control treatment for parental, WT Occ-expressing, and S471D Occ-expressing lines. Data are expressed as means ± SE ($n = 6$ to 8) and compared by using 2-way ANOVA with a Bonferroni *post hoc* test. *, $P < 0.05$ for parental versus S471D mutant-expressing lines at the indicated times.

staining) was significantly decreased in S471A Occ-expressing lines and increased in S471D Occ-expressing lines compared with lines expressing WT Occ (Fig. 1F and G). Together, these observations demonstrate that the expression of S471A Occ compromises TJ organization in a dominant manner.

TJ formation occurs after size-reductive proliferation. As detailed in the introduction, size-reductive proliferation is required for monolayer maturation. Here, the formation of TJs was examined across size-reductive proliferation and epithelial cell maturation. MDCK cells were plated onto 8 chambered slides at 162,500 cells/cm^2 (yielding confluence on the first day of plating). The cells underwent dramatic morphological changes associated with size-reductive proliferation in the first 3 days following confluence. Cell density increased by over 2-fold, as indicated by nucleus counts (Fig. 4A and B). Meanwhile, the AJs were partially completed by day 1 and largely formed by day 2, and the area within the AJ decreased by half by day 3 (Fig. 4C and D). Finally, TJ assembly assessed by ZO-1 staining was largely incomplete on day 1 but increased dramatically over days 2 and 3 such that colocalization with E-cadherin increased, indicating increased ZO-1 border localization (Fig. 4E and F). Packing was complete by 3 days postconfluence for each of the measured parameters, and no statistically significant changes occurred between days 3 and 4. The TJ organization observed in the S471A mutant-expressing lines appeared highly similar to that at the early time point in epithelial cell maturation; therefore, cell size and proliferation were examined in the mutant lines.

Size-reductive proliferation is attenuated by S471A Occ expression. Cell monolayers expressing S471A Occ were composed of fewer and larger cells than WT Occ- or S471D Occ-expressing monolayers (Fig. 5A to C). The number of nuclei was approximately half that of cells expressing WT Occ or the S471D mutant, and the area within the AJ (E-cadherin staining) was increased in S471A Occ-expressing confluent monolayers by 2- to 3-fold compared to WT Occ- or S471D Occ-expressing lines (Fig. 5A and B). To determine if S471A mutants altered cell proliferation, the cells were plated at a low density (1,400 cells/cm^2) and counted on days 1 to 4. The number of cells, as determined by flow analysis, was

reduced in S471A Occ-expressing monolayers at higher confluences on days 3 and 4 but not on day 1 or 2 when confluence was low and there was little cell contact, suggesting a loss of proliferation in a density-dependent manner (Fig. 5D). To further examine this possibility, we measured the proliferative rates of WT Occ-, S471A Occ-, and S471D Occ-expressing lines at various confluences by DNA synthesis measurements (Click-IT EdU). At 7,857 cells/cm^2 (~10% confluent) and 100,000 cells/cm^2 (~55% confluent), the number of cells with active DNA synthesis was measured over a 4-h period, whereas for plating of 185,714 cells/cm^2 (~100% confluent), the number of synthetically active cells was measured over 24 h since the rate of overall synthesis dramatically decreases as cells become more confluent. No difference in proliferation was observed at low confluence (Fig. 6A) but became increasingly evident with increasing confluence (Fig. 6B and C). When plated at ~100% confluence, fewer than 10% as many S471A Occ-expressing cells proliferated over 24 h (4 to 28 h postplating) compared to WT Occ-expressing cells, while there was no difference between WT Occ- and S471D Occ-expressing cells (Fig. 6C). The proliferation rate was near zero in all cell lines from 28 to 52 h postplating (Fig. 6D), suggesting that when plated at high confluence, proliferation is restricted in MDCK cells to a size-reductive or packing phase lasting no longer than 24 h, followed by relative quiescence. However, the expression of S471A Occ inhibits this packing phase. The transcriptional coactivator YAP promotes cell proliferation in the nucleus, and its nuclear exclusion marks the end of the Hippo signaling pathway and contributes to CIP (35). Despite proliferative quiescence, YAP localization remained nuclear in S471A Occ-expressing lines compared to WT Occ-expressing lines at quiescence, consistent with the S471A mutant stalling size-reductive proliferation and preventing YAP nuclear exclusion (Fig. 6E and F). Taken together, these results indicate that size-reductive proliferation is deficient in S471A Occ-expressing lines and raise the possibility of a connection between defective packing and poor TJ assembly (Fig. 1C).

Cell packing is necessary for barrier assembly. To evaluate the necessity of cell packing alone for barrier assembly, we treated parental MDCK cells with the Cdk inhibitor roscovitine starting at 24 h postplating to halt the cell cycle and size-reductive proliferation. The number of nuclei was decreased (Fig. 7A), and the area within the AJ was increased (Fig. 7B) compared to controls, confirming that packing was significantly attenuated. Transepithelial electrical resistance (TER) was decreased on day 3 (Fig. 7C), and there was a significant loss of ZO-1 border staining compared with continuous E-cadherin staining (Fig. 7D and E), indicating disorganization of TJ proteins at the border. These studies demonstrate that inhibition of cell packing alone reduces TJ assembly and prevents the formation of high resistance barriers.

S471A Occ compromises barrier function. The same loss of high resistance barriers was observed in S471A Occ-expressing lines with stalled size-reductive proliferation. WT Occ overexpression increased TER in mature (day 3 [Fig. 8A] and day 4 [Fig. 8B]) monolayers as well as after 12 h of reassembly following a Ca^{2+} switch experiment (Fig. 8C), as previously reported (36–38). No differences were evident between WT Occ- and S471D Occ-expressing lines at any of the time points. In contrast, S471A Occ expression reduced TER at all time points in all lines tested, and permeability to Ca^{2+}, K^+, and Cl^- ions was uniformly increased in S471A Occ mutants (Fig. 9A to C). Permeability to the small fluorescent molecule TAMRA (467 Da) was also increased in S471A mutant-expressing lines, and there was no difference between WT Occ-expressing, S471D mutant-expressing, and parental lines in TAMRA flux (Fig. 8D). These results indicate an increase in permeability to both ion and small-molecule flux in S471A Occ-expressing lines.

S471 is phosphorylated *in vitro* by G-protein-coupled receptor kinase (GRK), and GRK inhibitors attenuate epithelial cell maturation. Our previous studies suggest that S471 phosphorylation is important for cell packing and barrier formation. To screen potential cellular kinases for this residue, putative kinases

A

IC_{50} (μM)		
GRK Inhib 22	ABMH	Paroxetine
0.95 ± 0.12	499.00 ± 144.00	78.80 ± 12.30

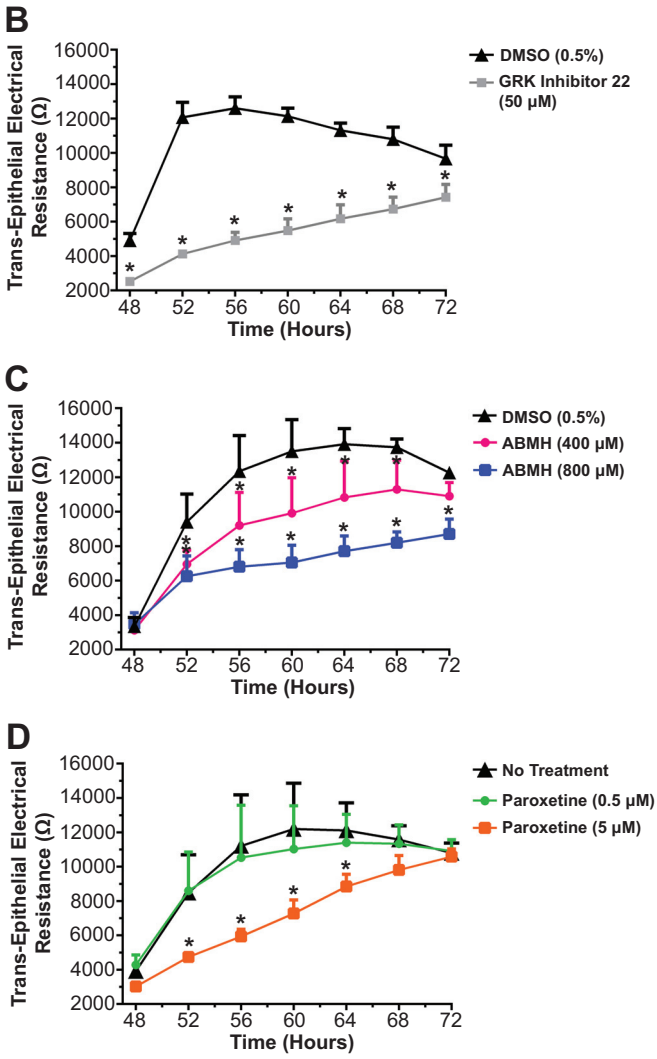

FIG 12 GRK inhibitor activities and effect on TER. (A) *In vitro* IC_{50}s for GRK inhibitors. (B to D) Day 3 TER composite traces from ECIS measures for various GRK inhibitors, including GRK inhibitor 22 (B), ABMH (C), and paroxetine (D). Data are expressed as means ± SD ($n = 6$ [A] and $n = 4$ to 8 [B to D]). *, $P < 0.05$ compared to DMSO (0.5%) or no treatment.

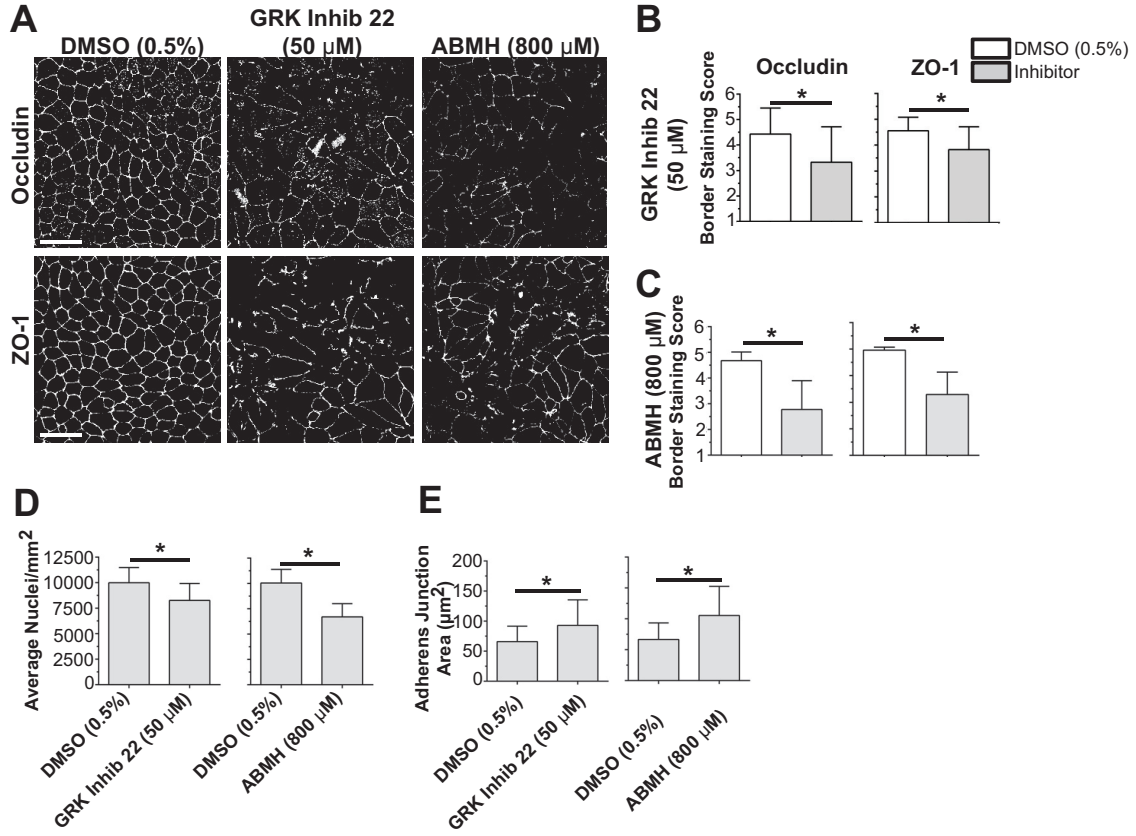

FIG 13 GRK inhibitors decrease TJ border staining and cell number and increase cell size. (A) IF maximum projected images of total occludin and ZO-1 from DMSO control-, GRK Inhib 22-, and ABMH-treated parental MDCK cells (bar = 50 μm). (B and C) Semiquantitative scoring (see Materials and Methods) of occludin and ZO-1 border continuity following GRK Inhib 22 (B) or ABMH (C) treatment. (D and E) Nucleus counts (D) and quantification of the area within the AJ (E) of DMSO control- versus GRK Inhib 22- or ABMH-treated parental MDCK cells. Drug was present from the beginning of each run and replenished every 24 h along with fresh medium (averages from 14 [B and C] or 4 [D and E] images per condition). *, $P < 0.05$ compared to WT Occ or the DMSO control.

were identified by using three kinase prediction software programs, and kinases predicted by at least two programs were screened against a 21-amino-acid (aa) peptide with S471 at the center (Fig. 10) (see Materials and Methods). This peptide was phosphorylated *in vitro* by members of the polo-like kinase (PLK), calcium/calmodulin-dependent kinase (CaMKII), and GRK families (Fig. 10). Since GRK was previously implicated in cell size control (39), and GRK isoforms were present in MDCK cells (Fig. 11A), this kinase was targeted for cell packing and junction formation studies. Small interfering RNAs (siRNAs) for GRK were unsuccessful in knocking down protein levels despite multiple attempts. However, three chemically distinct pharmacological GRK inhibitors prevented epithelial cell maturation. GRK Inhib 22 (CCG215022), a potent GRK inhibitor (32), demonstrated inhibition of GRK6 with a 50% inhibitory concentration (IC_{50}) of 0.95 ± 0.12 μM, while 4-amino-5-(bromomethyl)-2-methylpyrimidine hydrobromide (ABMH) and paroxetine (40) inhibited GRK6 with IC_{50}s of 499 ± 144 μM and 78.80 ± 12.30 μM, respectively (Fig. 12A). MDCK cells were plated at confluence and treated with a GRK inhibitor upon cell feeding every 24 h. Occludin and ZO-1 localizations at the border were reduced on day 3 following treatment of parental MDCK cells with GRK Inhib 22 (Fig. 13A and B) or ABMH (Fig. 13A and C) compared with a dimethyl sulfoxide (DMSO) control. Cell packing was attenuated by both inhibitors, as demonstrated by a decrease in the number of nuclei (Fig. 13D) and an increase in the area within the AJ (Fig. 13E). TER was measured in parental cells treated with GRK inhibitors. Treatment with all three GRK inhibitors reduced day 3 TER and delayed barrier development in a dose-dependent manner, yielding reduced TER on day 3 (Fig. 11B to E and 12B to D). Cell viability was not decreased with any of the inhibitors (Fig. 14). In contrast to the panspecific GRK Inhib 22, inhibitors specific to the GRK2-3 subfamily (GRK Inhib 63 and GRK Inhib 64) did not reduce TER (Fig. 11B). Importantly, overexpression of S471D Occ was sufficient to attenuate the GRK Inhib 22-mediated TER decrease in parental MDCK cells, while WT Occ expression tended to normalize TER but was not statistically significant (Fig. 11F). These results strongly implicate GRK isoforms in the phosphorylation of occludin S471 and demonstrate that the inhibition of GRK isoforms significantly decreases cell packing, TJ assembly, and peak TER, which may be attenuated by the expression of the S471D Occ phosphomimetic.

DISCUSSION

Despite the importance of barrier formation and dysfunction in a variety of diseases (41–43), the series of events leading to barrier maturation remain incompletely characterized. The present study demonstrates the necessity of size-reductive proliferation or cell

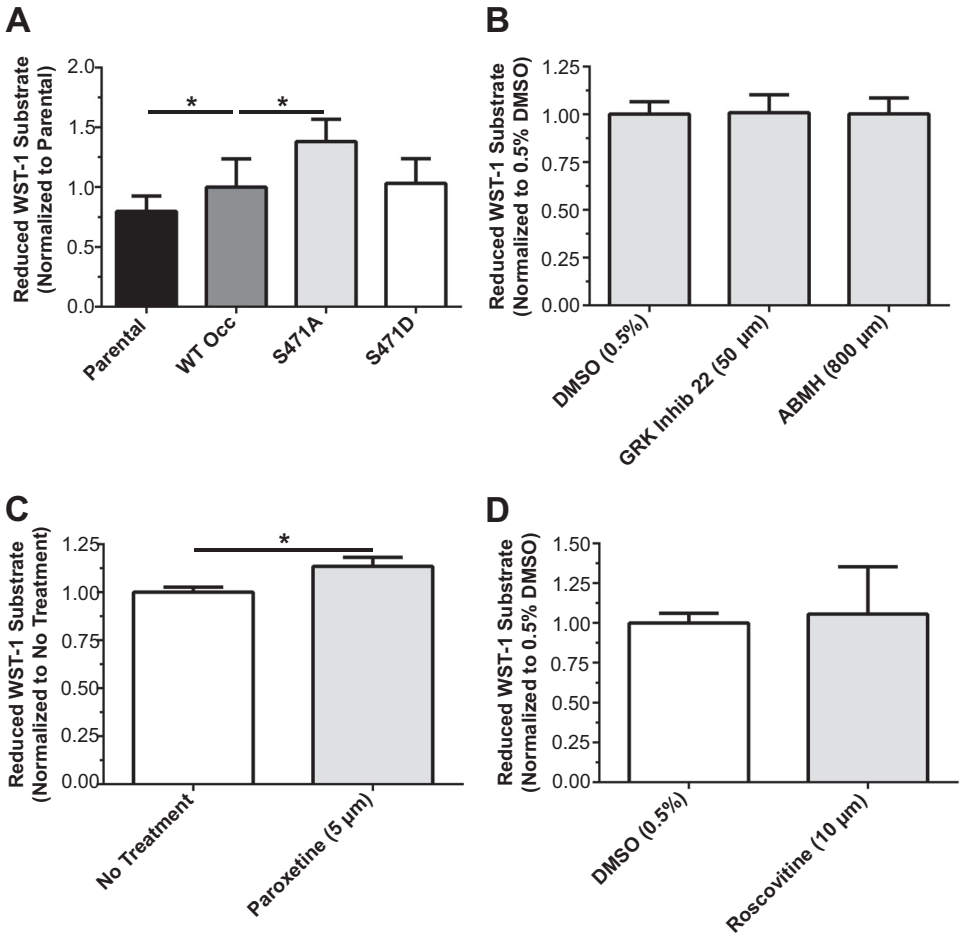

FIG 14 Cell viability is not decreased by occludin overexpression or the tested pharmacological agents. Shown is quantification of WST-1 reduction as a measure of viability for parental and occludin-overexpressing cell lines (A), GRK Inhib 22 and ABMH GRK inhibitors (B), the GRK inhibitor paroxetine (C), and the cell cycle inhibitor roscovitine (D). Data are expressed as means ± SD ($n = 8$). *, $P < 0.05$ compared to WT Occ, 0.5% DMSO, or no treatment.

packing for normal barrier maturation and identifies a role for the TJ protein occludin in this process. Previous studies demonstrated that occludin contributes to growth control and cell cycle progression (15, 20), is altered in epithelial cancers (44, 45), and may act as a tumor suppressor (20). Evidence is presented here demonstrating that the phosphorylation of S471 of occludin regulates entry into size-reductive proliferation after cell contact. Expression of an S471-phosphoinhibitory mutant, Occ S471A, acts in a dominant manner to attenuate cell packing and subsequent TJ maturation and the formation of high-resistance barriers. These effects can be recapitulated by treating confluent monolayers with a cell cycle inhibitor, demonstrating the necessity of cell packing for complete TJ assembly and monolayer maturation. Finally, Occ S471 was found to be a substrate for GRK, and three separate GRK inhibitors attenuated epithelial cell maturation. These data suggest that GRK phosphorylation of Occ S471 signals to allow size-reductive proliferation. The reduced cell size then relieves cytoskeletal strain, promoting Hippo signaling for YAP nuclear exclusion (7) and cellular quiescence with completed TJ formation. The inhibition of S471 phosphorylation or prevention of cell cycle progression postconfluence prevents size-reductive proliferation, leading to fewer, larger cells with incomplete TJ formation (Fig. 15).

TJ barrier regulation by occludin is dependent on phosphosites, which are particularly abundant in the C-terminal coiled coil (46). Occludin dephosphorylation is associated with decreased electrical resistance and localization of occludin at the membrane, and C-terminal deletion increases solute flux and attenuates TJ organization (36, 47). Specific phosphosites regulate the occludin-mediated response to various growth factors and cytokines. For example, phosphorylation at S490 by protein kinase CβII (PKCβII) in response to vascular endothelial growth factor treatment increases occludin ubiquitination, leading to endocytosis and increased permeability (42, 48). S490 phosphorylation also facilitates mitotic entry and increases proliferation (15). Phosphorylation at S408 mediates interleukin-13-induced barrier loss, and inhibition of the S408 kinase CK2 increases TER through altered intermolecular complex formation within the TJ (49). Specific occludin phosphosites also regulate occludin's interaction with other TJ proteins, suggesting additional points of regulation (50–52). These studies support a role for specific occludin phosphosites in barrier regulation and suggest that novel sites may have important regulatory roles.

Overexpression of nonphosphorylatable S471A Occ disrupted cell packing and maturation of TJs but not AJs. AJs are formed prior to TJs following cell-cell contact, and while TJ and cytoskel-

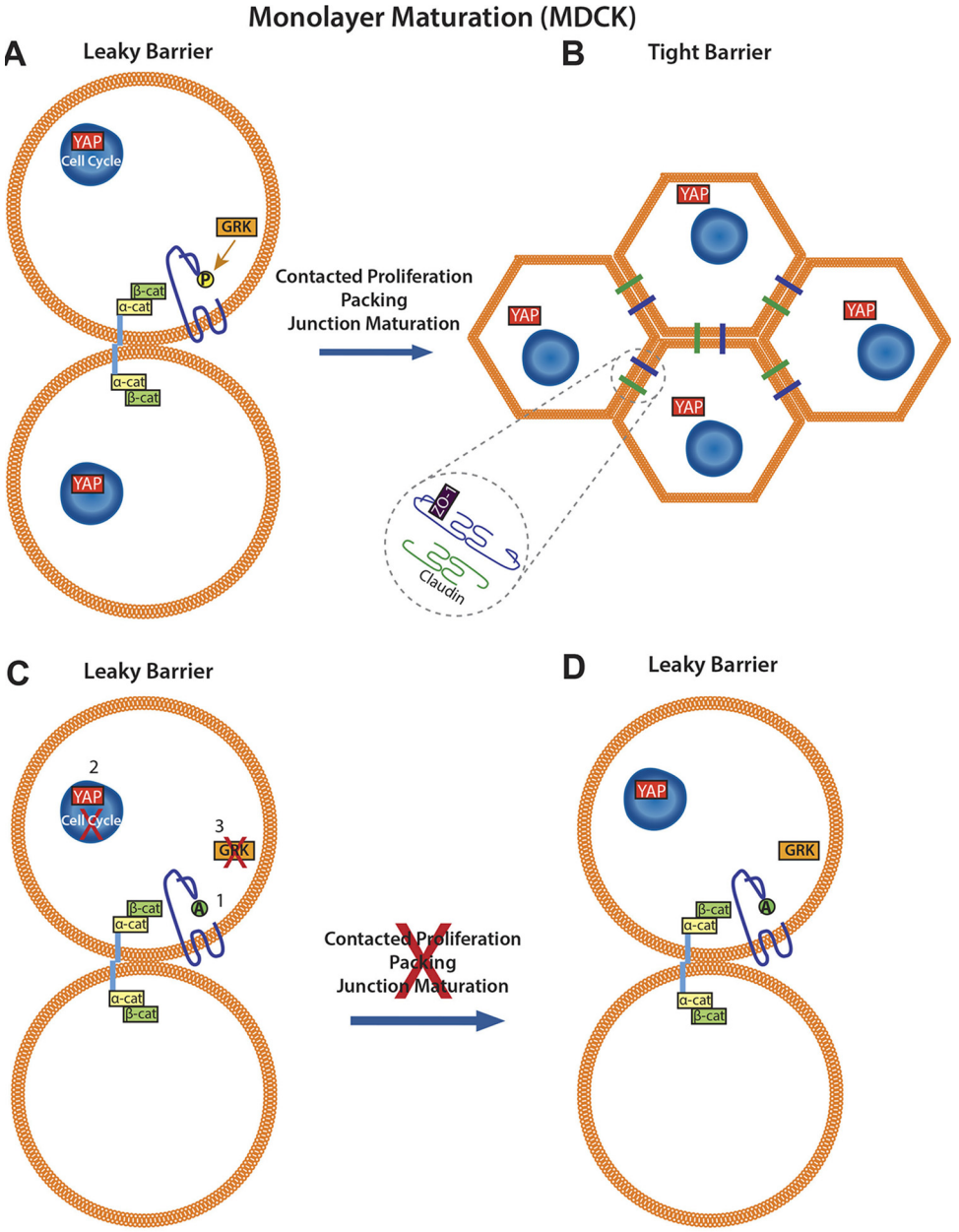

FIG 15 Model of the contribution of occludin S471 to monolayer maturation. (A) Increasing confluence leads to contact by E-cadherin extracellular domains of adjacent cells (blue bars). Cell confluence continues to increase, and occludin S471 is phosphorylated by GRK, allowing size-reductive proliferation, decreasing cell area, and increasing cell number. (B) As size-reductive proliferation progresses, YAP becomes excluded from the nucleus, and junctional maturation proceeds, yielding a mature monolayer with high barrier resistance and proliferative quiescence. (C) Monolayer maturation may be perturbed by Ser-to-Ala mutation of occludin at S471 (1), cell cycle inhibition of confluent monolayers (roscovitine) (2), or inhibition of the S471 kinase GRK (GRK Inhib 22, ABMH, and paroxetine) (3). (D) In all cases, size-reductive proliferation is inhibited, leaving an immature monolayer with complete adherens junction formation but nuclear YAP, poor TJ organization, and low TER.

etal organization were decreased in a dominant fashion in S471A Occ-expressing lines, AJ assembly was unaffected, revealing that AJ formation does not require cell packing as TJ formation does. Furthermore, GRK inhibition did not alter AJ formation. Additionally, S471A Occ-expressing monolayers were composed of fewer cells with increased area, suggesting premature proliferative cessation. The Hippo signaling pathway is an important determinant of cell and organ sizes, and nuclear exclusion of the coactivator YAP accompanies proliferative quiescence. While YAP is just one of several nuclear Hippo proteins, proliferative cessation in S471A Occ-expressing cell lines despite continued nuclear YAP localization indicates a dominant effect of the mutant, leading to the premature arrest of packing prior to the completion of the Hippo signaling pathway.

S471A Occ expression reduced TER despite similar TJ protein expression and Ca^{2+}, K^{+}, and Cl^{-} ion permeability in all lines (Fig. 2 and 9), suggesting nonspecific flux from gaps in the TJ rather than an altered expression of claudins or claudin pore for-

mation to induce changes in the permeability of a specific ion. Importantly, packing deficiencies evident in S471A Occ-expressing lines, including mislocalized TJ proteins and reduced TER, were recapitulated by pharmacological inhibition of packing alone, indicating that packing is necessary for establishing anatomically and functionally normal barriers. It is noteworthy that many TJ proteins appear at the cell border upon contact and before packing but that a continuous apical TJ is not completed until after size-reductive proliferation and quiescence. How these downstream events are regulated remains an area for future investigation.

Structural analysis of occludin and ZO-1 binding suggests that occludin S471 is located within the acidic head of the coiled coil that specifically binds the GuK domain of ZO-1 (22), raising the possibility that occludin S471 phosphorylation affects the conformation of ZO-1 and thus epithelial cell maturation. The ZO family acts to organize cell junctions and links the junction to the actin cytoskeleton (53). Changes in the localization of all the TJ proteins analyzed in the S471A Occ mutants as well as altered actin organization, particularly at the cortical ring, are consistent with an alteration in proper ZO-1 function at the cell membrane. Occludin expression is not necessary for TJ formation in the intestinal epithelia of mice or in MDCK cells (13, 54), suggesting that the regulatory effect of occludin may eventually be compensated for in its absence. However, the effect of the S471A mutation was not transient, indicating that the presence of nonphosphorylatable S471 occludin inhibits packing and TJ formation in a dominant manner and revealing this site as a regulator of size-reductive proliferation and epithelial cell maturation.

GRKs can phosphorylate S471 Occ, and inhibition of GRKs recapitulates results obtained with S471A Occ-expressing lines and cell cycle inhibition. GRKs contribute to signal transduction desensitization by phosphorylating G-protein-coupled receptors and preventing coupling with cytoplasmic G proteins. The sequence surrounding Occ S471 was tested with multiple kinase prediction software programs, and 41 kinases were selected for screening. GRK family members were able to phosphorylate the Occ S471-containing peptide, consistent with recent studies demonstrating that non-G-protein-coupled receptor proteins, including cytoskeletal (39), nuclear (55), and membrane (56) proteins as well as transcription factors (57), can be GRK substrates. Seven GRK isoforms have been identified and are divided into three subfamilies based on sequence homology: isoforms 1 and 7 are tissue specific to the eye, while isoforms 2 and 3 are ubiquitously expressed, as are isoforms 5 and 6, while isoform 4 has limited expression (58). Importantly, three structurally distinct GRK inhibitors were able to recapitulate deficiencies in packing and TJ protein localization evident in S471A Occ-expressing lines in a dose-dependent manner. In contrast to the panspecific GRK Inhib 22, two inhibitors with greater specificity for the GRK2-3 subfamily did not decrease TER. This result along with a lack of GRK1 and -7 expression in kidney and the confirmed expression of the GRK4-6 subfamily in MDCK cells by Western blotting suggests that at least one member of the GRK4-6 subfamily is an S471 kinase in MDCK cells. Silencing of GRK5 increases cell area, decreases tumor size (39), and attenuates proliferation in various cancer lines (59, 60), demonstrating a regulatory role for the GRK4-6 subfamily in cell size and proliferation. While there are likely off-target effects of the GRK inhibitors used in the present experiments, the ability of three structurally distinct inhibitors to induce the same effect, preventing epithelial cell maturation, strongly suggests that GRK is the target. Critically, the GRK inhibitor-mediated TER decrease observed in parental MDCK cells was significantly attenuated in phosphomimetic S471D Occ-overexpressing cells, implicating Occ S471 as a critical GRK target in epithelial cell maturation.

Taken together, these observations support a model in which Occ S471 phosphorylation contributes to the regulation of entry into size-reductive proliferation after contact, followed by epithelial quiescence and the assembly of TJs at the cell border, leading to a high resistance barrier and a mature monolayer. These findings extend the current understanding of the role of occludin and establish the importance of cell packing in barrier formation.

ACKNOWLEDGMENTS

We acknowledge Tiffany Frey for cell line development, Bret Hughes for the use of equipment and expertise in ion permeability studies, John Tesmer for insight into GRK inhibitors, David Murrel for the design of schematics, and Stephen Lentz for technical assistance with confocal imaging and quantification.

FUNDING INFORMATION

This work, including the efforts of John M. Flanagan and David A. Antonetti, was funded by HHS | NIH | National Institute of General Medical Sciences (NIGMS) (GM094526). This work, including the efforts of David A. Antonetti, was funded by Research to Prevent Blindness (RPB). This work, including the efforts of David A. Antonetti, was funded by HHS | NIH | National Eye Institute (NEI) (EY012021). This work, including the efforts of David A. Antonetti, was funded by HHS | NIH | National Eye Institute (NEI) (P30 EY007003).

REFERENCES

1. **Li S, Gerrard ER, Jr, Balkovetz DF.** 2004. Evidence for ERK1/2 phosphorylation controlling contact inhibition of proliferation in Madin-Darby canine kidney epithelial cells. Am J Physiol Cell Physiol **287:**C432–C439. http://dx.doi.org/10.1152/ajpcell.00020.2004.
2. **Puliafito A, Hufnagel L, Neveu P, Streichan S, Sigal A, Fygenson DK, Shraiman BI.** 2012. Collective and single cell behavior in epithelial contact inhibition. Proc Natl Acad Sci U S A **109:**739–744. http://dx.doi.org/10.1073/pnas.1007809109.
3. **Kim NG, Koh E, Chen X, Gumbiner BM.** 2011. E-cadherin mediates contact inhibition of proliferation through Hippo signaling-pathway components. Proc Natl Acad Sci U S A **108:**11930–11935. http://dx.doi.org/10.1073/pnas.1103345108.
4. **Levine EM, Becker Y, Boone CW, Eagle H.** 1965. Contact inhibition, macromolecular synthesis, and polyribosomes in cultured human diploid fibroblasts. Proc Natl Acad Sci U S A **53:**350–356. http://dx.doi.org/10.1073/pnas.53.2.350.
5. **Adam G, Steiner U, Maier H, Ullrich S.** 1982. Analysis of cellular interactions in density-dependent inhibition of 3T3 cell proliferation. Biophys Struct Mech **9:**75–82. http://dx.doi.org/10.1007/BF00539104.
6. **Erlinger SU, Saier MH, Jr.** 1982. Decrease in protein content and cell volume of cultured dog kidney epithelial cells during growth. In Vitro **18:**196–202. http://dx.doi.org/10.1007/BF02618571.
7. **Aragona M, Panciera T, Manfrin A, Giulitti S, Michielin F, Elvassore N, Dupont S, Piccolo S.** 2013. A mechanical checkpoint controls multicellular growth through YAP/TAZ regulation by actin-processing factors. Cell **154:**1047–1059. http://dx.doi.org/10.1016/j.cell.2013.07.042.
8. **Rauskolb C, Sun S, Sun G, Pan Y, Irvine KD.** 2014. Cytoskeletal tension inhibits Hippo signaling through an Ajuba-Warts complex. Cell **158:**143–156. http://dx.doi.org/10.1016/j.cell.2014.05.035.
9. **Trepat X, Wasserman MR, Angelini TE, Millet E, Weitz DA, Butler JP, Fredberg JJ.** 2009. Physical forces during collective cell migration. Nat Phys Lett **5:**426–430. http://dx.doi.org/10.1038/nphys1269.
10. **Anderson JM, Van Itallie CM.** 2009. Physiology and function of the tight

junction. Cold Spring Harb Perspect Biol **1:**a002584. http://dx.doi.org/10.1101/cshperspect.a002584.
11. **Furuse M, Hirase T, Itoh M, Nagafuchi A, Yonemura S, Tsukita S, Tsukita S.** 1993. Occludin: a novel integral membrane protein localizing at tight junctions. J Cell Biol **123:**1777–1788. http://dx.doi.org/10.1083/jcb.123.6.1777.
12. **Saitou M, Furuse M, Sasaki H, Schulzke JD, Fromm M, Takano H, Noda T, Tsukita S.** 2000. Complex phenotype of mice lacking occludin, a component of tight junction strands. Mol Biol Cell **11:**4131–4142. http://dx.doi.org/10.1091/mbc.11.12.4131.
13. **Schulzke JD, Gitter AH, Mankertz J, Spiegel S, Seidler U, Amasheh S, Saitou M, Tsukita S, Fromm M.** 2005. Epithelial transport and barrier function in occludin-deficient mice. Biochim Biophys Acta **1669:**34–42. http://dx.doi.org/10.1016/j.bbamem.2005.01.008.
14. **O'Driscoll MC, Daly SB, Urquhart JE, Black GC, Pilz DT, Brockmann K, McEntagart M, Abdel-Salam G, Zaki M, Wolf NI, Ladda RL, Sell S, D'Arrigo S, Squier W, Dobyns WB, Livingston JH, Crow YJ.** 2010. Recessive mutations in the gene encoding the tight junction protein occludin cause band-like calcification with simplified gyration and polymicrogyria. Am J Hum Genet **87:**354–364. http://dx.doi.org/10.1016/j.ajhg.2010.07.012.
15. **Runkle EA, Sundstrom JM, Runkle KB, Liu X, Antonetti DA.** 2011. Occludin localizes to centrosomes and modifies mitotic entry. J Biol Chem **286:**30847–30858. http://dx.doi.org/10.1074/jbc.M111.262857.
16. **Rachow S, Zorn-Kruppa M, Ohnemus U, Kirschner N, Vidal-y-Sy S, von den Driesch P, Bornchen C, Eberle J, Mildner M, Vettorazzi E, Rosenthal R, Moll I, Brandner JM.** 2013. Occludin is involved in adhesion, apoptosis, differentiation and Ca2+-homeostasis of human keratinocytes: implications for tumorigenesis. PLoS One **8:**e55116. http://dx.doi.org/10.1371/journal.pone.0055116.
17. **Tobioka H, Isomura H, Kokai Y, Tokunaga Y, Yamaguchi J, Sawada N.** 2004. Occludin expression decreases with the progression of human endometrial carcinoma. Hum Pathol **35:**159–164. http://dx.doi.org/10.1016/j.humpath.2003.09.013.
18. **Martin TA, Mansel RE, Jiang WG.** 2010. Loss of occludin leads to the progression of human breast cancer. Int J Mol Med **26:**723–734.
19. **Osanai M, Murata M, Nishikiori N, Chiba H, Kojima T, Sawada N.** 2006. Epigenetic silencing of occludin promotes tumorigenic and metastatic properties of cancer cells via modulations of unique sets of apoptosis-associated genes. Cancer Res **66:**9125–9133. http://dx.doi.org/10.1158/0008-5472.CAN-06-1864.
20. **Wang Z, Mandell KJ, Parkos CA, Mrsny RJ, Nusrat A.** 2005. The second loop of occludin is required for suppression of Raf1-induced tumor growth. Oncogene **24:**4412–4420. http://dx.doi.org/10.1038/sj.onc.1208634.
21. **Sundstrom JM, Tash BR, Murakami T, Flanagan JM, Bewley MC, Stanley BA, Gonsar KB, Antonetti DA.** 2009. Identification and analysis of occludin phosphosites: a combined mass spectrometry and bioinformatics approach. J Proteome Res **8:**808–817. http://dx.doi.org/10.1021/pr7007913.
22. **Tash BR, Bewley MC, Russo M, Keil JM, Griffin KA, Sundstrom JM, Antonetti DA, Tian F, Flanagan JM.** 2012. The occludin and ZO-1 complex, defined by small angle X-ray scattering and NMR, has implications for modulating tight junction permeability. Proc Natl Acad Sci U S A **109:**10855–10860. http://dx.doi.org/10.1073/pnas.1121390109.
23. **Lye MF, Fanning AS, Su Y, Anderson JM, Lavie A.** 2010. Insights into regulated ligand binding sites from the structure of ZO-1 Src homology 3-guanylate kinase module. J Biol Chem **285:**13907–13917. http://dx.doi.org/10.1074/jbc.M109.093674.
24. **Rodgers LS, Beam MT, Anderson JM, Fanning AS.** 2013. Epithelial barrier assembly requires coordinated activity of multiple domains of the tight junction protein ZO-1. J Cell Sci **126:**1565–1575. http://dx.doi.org/10.1242/jcs.113399.
25. **Umeda K, Ikenouchi J, Katahira-Tayama S, Furuse K, Sasaki H, Nakayama M, Matsui T, Tsukita S, Furuse M, Tsukita S.** 2006. ZO-1 and ZO-2 independently determine where claudins are polymerized in tight-junction strand formation. Cell **126:**741–754. http://dx.doi.org/10.1016/j.cell.2006.06.043.
26. **Zhu J, Shang Y, Xia C, Wang W, Wen W, Zhang M.** 2011. Guanylate kinase domains of the MAGUK family scaffold proteins as specific phospho-protein-binding modules. EMBO J **30:**4986–4997. http://dx.doi.org/10.1038/emboj.2011.428.
27. **Shen L, Turner JR.** 2005. Actin depolymerization disrupts tight junctions via caveolae-mediated endocytosis. Mol Biol Cell **16:**3919–3936. http://dx.doi.org/10.1091/mbc.E04-12-1089.
28. **Phillips BE, Cancel L, Tarbell JM, Antonetti DA.** 2008. Occludin independently regulates permeability under hydrostatic pressure and cell division in retinal pigment epithelial cells. Invest Ophthalmol Vis Sci **49:**2568–2576. http://dx.doi.org/10.1167/iovs.07-1204.
29. **Xue Y, Ren J, Gao X, Jin C, Wen L, Yao X.** 2008. GPS 2.0, a tool to predict kinase-specific phosphorylation sites in hierarchy. Mol Cell Proteomics **7:**1598–1608. http://dx.doi.org/10.1074/mcp.M700574-MCP200.
30. **Huang HD, Lee TY, Tzeng SW, Horng JT.** 2005. KinasePhos: a Web tool for identifying protein kinase-specific phosphorylation sites. Nucleic Acids Res **33:**W226–W229. http://dx.doi.org/10.1093/nar/gki471.
31. **Blom N, Gammeltoft S, Brunak S.** 1999. Sequence and structure-based prediction of eukaryotic protein phosphorylation sites. J Mol Biol **294:**1351–1362. http://dx.doi.org/10.1006/jmbi.1999.3310.
32. **Homan KT, Waldschmidt HV, Glukhova A, Cannavo A, Song J, Cheung JY, Koch WJ, Larsen SD, Tesmer JJ.** 2015. Crystal structure of G protein-coupled receptor kinase 5 in complex with a rationally designed inhibitor. J Biol Chem **290:**20649–20659. http://dx.doi.org/10.1074/jbc.M115.647370.
33. **Titchenell PM, Lin CM, Keil JM, Sundstrom JM, Smith CD, Antonetti DA.** 2012. Novel atypical PKC inhibitors prevent vascular endothelial growth factor-induced blood-retinal barrier dysfunction. Biochem J **446:**455–467. http://dx.doi.org/10.1042/BJ20111961.
34. **Hou J, Paul DL, Goodenough DA.** 2005. Paracellin-1 and the modulation of ion selectivity of tight junctions. J Cell Sci **118:**5109–5118. http://dx.doi.org/10.1242/jcs.02631.
35. **Gumbiner BM, Kim NG.** 2014. The Hippo-YAP signaling pathway and contact inhibition of growth. J Cell Sci **127:**709–717. http://dx.doi.org/10.1242/jcs.140103.
36. **Balda MS, Whitney JA, Flores C, Gonzalez S, Cereijido M, Matter K.** 1996. Functional dissociation of paracellular permeability and transepithelial electrical resistance and disruption of the apical-basolateral intramembrane diffusion barrier by expression of a mutant tight junction membrane protein. J Cell Biol **134:**1031–1049. http://dx.doi.org/10.1083/jcb.134.4.1031.
37. **McCarthy KM, Skare IB, Stankewich MC, Furuse M, Tsukita S, Rogers RA, Lynch RD, Schneeberger EE.** 1996. Occludin is a functional component of the tight junction. J Cell Sci **109**(Part 9):2287–2298.
38. **Van Itallie CM, Fanning AS, Holmes J, Anderson JM.** 2010. Occludin is required for cytokine-induced regulation of tight junction barriers. J Cell Sci **123:**2844–2852. http://dx.doi.org/10.1242/jcs.065581.
39. **Chakraborty PK, Zhang Y, Coomes AS, Kim WJ, Stupay R, Lynch LD, Atkinson T, Kim JI, Nie Z, Daaka Y.** 2014. G protein-coupled receptor kinase GRK5 phosphorylates moesin and regulates metastasis in prostate cancer. Cancer Res **74:**3489–3500. http://dx.doi.org/10.1158/0008-5472.CAN-13-2708.
40. **Thal DM, Homan KT, Chen J, Wu EK, Hinkle PM, Huang ZM, Chuprun JK, Song J, Gao E, Cheung JY, Sklar LA, Koch WJ, Tesmer JJ.** 2012. Paroxetine is a direct inhibitor of G protein-coupled receptor kinase 2 and increases myocardial contractility. ACS Chem Biol **7:**1830–1839. http://dx.doi.org/10.1021/cb3003013.
41. **Morgan DH, Ghribi O, Hui L, Geiger JD, Chen X.** 2014. Cholesterol-enriched diet disrupts the blood-testis barrier in rabbits. Am J Physiol Endocrinol Metab **307:**E1125–E1130. http://dx.doi.org/10.1152/ajpendo.00416.2014.
42. **Murakami T, Frey T, Lin C, Antonetti DA.** 2012. Protein kinase cbeta phosphorylates occludin regulating tight junction trafficking in vascular endothelial growth factor-induced permeability in vivo. Diabetes **61:**1573–1583. http://dx.doi.org/10.2337/db11-1367.
43. **Schmitz H, Barmeyer C, Fromm M, Runkel N, Foss HD, Bentzel CJ, Riecken EO, Schulzke JD.** 1999. Altered tight junction structure contributes to the impaired epithelial barrier function in ulcerative colitis. Gastroenterology **116:**301–309. http://dx.doi.org/10.1016/S0016-5085(99)70126-5.
44. **Gonzalez-Mariscal L, Lechuga S, Garay E.** 2007. Role of tight junctions in cell proliferation and cancer. Prog Histochem Cytochem **42:**1–57. http://dx.doi.org/10.1016/j.proghi.2007.01.001.
45. **Runkle EA, Mu D.** 2013. Tight junction proteins: from barrier to tumorigenesis. Cancer Lett **337:**41–48. http://dx.doi.org/10.1016/j.canlet.2013.05.038.
46. **Cummins PM.** 2012. Occludin: one protein, many forms. Mol Cell Biol **32:**242–250. http://dx.doi.org/10.1128/MCB.06029-11.

47. **Andreeva AY, Krause E, Muller EC, Blasig IE, Utepbergenov DI.** 2001. Protein kinase C regulates the phosphorylation and cellular localization of occludin. J Biol Chem **276:**38480–38486. http://dx.doi.org/10.1074/jbc.M104923200.
48. **Murakami T, Felinski EA, Antonetti DA.** 2009. Occludin phosphorylation and ubiquitination regulate tight junction trafficking and vascular endothelial growth factor-induced permeability. J Biol Chem **284:**21036–21046. http://dx.doi.org/10.1074/jbc.M109.016766.
49. **Raleigh DR, Boe DM, Yu D, Weber CR, Marchiando AM, Bradford EM, Wang Y, Wu L, Schneeberger EE, Shen L, Turner JR.** 2011. Occludin S408 phosphorylation regulates tight junction protein interactions and barrier function. J Cell Biol **193:**565–582. http://dx.doi.org/10.1083/jcb.201010065.
50. **Dorfel MJ, Westphal JK, Bellmann C, Krug SM, Cording J, Mittag S, Tauber R, Fromm M, Blasig IE, Huber O.** 2013. CK2-dependent phosphorylation of occludin regulates the interaction with ZO-proteins and tight junction integrity. Cell Commun Signal **11:**40. http://dx.doi.org/10.1186/1478-811X-11-40.
51. **Elias BC, Suzuki T, Seth A, Giorgianni F, Kale G, Shen L, Turner JR, Naren A, Desiderio DM, Rao R.** 2009. Phosphorylation of Tyr-398 and Tyr-402 in occludin prevents its interaction with ZO-1 and destabilizes its assembly at the tight junctions. J Biol Chem **284:**1559–1569. http://dx.doi.org/10.1074/jbc.M804783200.
52. **Suzuki T, Elias BC, Seth A, Shen L, Turner JR, Giorgianni F, Desiderio D, Guntaka R, Rao R.** 2009. PKC eta regulates occludin phosphorylation and epithelial tight junction integrity. Proc Natl Acad Sci U S A **106:**61–66. http://dx.doi.org/10.1073/pnas.0802741106.
53. **Gonzalez-Mariscal L, Betanzos A, Avila-Flores A.** 2000. MAGUK proteins: structure and role in the tight junction. Semin Cell Dev Biol **11:**315–324. http://dx.doi.org/10.1006/scdb.2000.0178.
54. **Yu AS, McCarthy KM, Francis SA, McCormack JM, Lai J, Rogers RA, Lynch RD, Schneeberger EE.** 2005. Knockdown of occludin expression leads to diverse phenotypic alterations in epithelial cells. Am J Physiol Cell Physiol **288:**C1231–C1241. http://dx.doi.org/10.1152/ajpcell.00581.2004.
55. **Martini JS, Raake P, Vinge LE, DeGeorge BR, Jr, Chuprun JK, Harris DM, Gao E, Eckhart AD, Pitcher JA, Koch WJ.** 2008. Uncovering G protein-coupled receptor kinase-5 as a histone deacetylase kinase in the nucleus of cardiomyocytes. Proc Natl Acad Sci U S A **105:**12457–12462. http://dx.doi.org/10.1073/pnas.0803153105.
56. **Dinudom A, Fotia AB, Lefkowitz RJ, Young JA, Kumar S, Cook DI.** 2004. The kinase Grk2 regulates Nedd4/Nedd4-2-dependent control of epithelial Na+ channels. Proc Natl Acad Sci U S A **101:**11886–11890. http://dx.doi.org/10.1073/pnas.0402178101.
57. **Patial S, Luo J, Porter KJ, Benovic JL, Parameswaran N.** 2010. G-protein-coupled-receptor kinases mediate TNFalpha-induced NFkappaB signalling via direct interaction with and phosphorylation of IkappaBalpha. Biochem J **425:**169–178. http://dx.doi.org/10.1042/BJ20090908.
58. **Gurevich EV, Tesmer JJ, Mushegian A, Gurevich VV.** 2012. G protein-coupled receptor kinases: more than just kinases and not only for GPCRs. Pharmacol Ther **133:**40–69. http://dx.doi.org/10.1016/j.pharmthera.2011.08.001.
59. **Kaur G, Kim J, Kaur R, Tan I, Bloch O, Sun MZ, Safaee M, Oh MC, Sughrue M, Phillips J, Parsa AT.** 2013. G-protein coupled receptor kinase (GRK)-5 regulates proliferation of glioblastoma-derived stem cells. J Clin Neurosci **20:**1014–1018. http://dx.doi.org/10.1016/j.jocn.2012.10.008.
60. **Kim JI, Chakraborty P, Wang Z, Daaka Y.** 2012. G-protein coupled receptor kinase 5 regulates prostate tumor growth. J Urol **187:**322–329. http://dx.doi.org/10.1016/j.juro.2011.09.049.